Probing the symmetry of atomic wavefunctions from the point of view of strong field-driven electrons

2010 New J. Phys. 12 073032

(http://iopscience.iop.org/1367-2630/12/7/073032)

New Journal of Physics
The open-access journal for physics

Probing the symmetry of atomic wavefunctions from the point of view of strong field-driven electrons

D Shafir[1,5], Y Mairesse[2], H J Wörner[3], K Rupnik[4], D M Villeneuve[3], P B Corkum[3] and N Dudovich[1]

[1] Department of Physics of Complex Systems, Weizmann Institute of Science, Rehovot 76100, Israel
[2] CELIA, Université Bordeaux I, UMR 5107 (CNRS, Bordeaux 1, CEA), 351 Cours de la Libération, 33405 Talence Cedex, France
[3] National Research Council of Canada, 100 Sussex Drive, Ottawa, Ontario K1A 0R6, Canada
[4] Department of Chemistry, Louisiana State University, Baton Rouge, LO 70803-1804, USA
E-mail: dror.shafir@weizmann.ac.il

New Journal of Physics **12** (2010) 073032 (16pp)
Received 30 September 2009
Published 26 July 2010
Online at http://www.njp.org/
doi:10.1088/1367-2630/12/7/073032

Abstract. In this paper, we analyze a new approach that was first presented by Shafir *et al* (2009 *Nat. Phys.* **5** 412–6) to probe the symmetry of atomic wavefunctions via the high harmonic generation process. In this scheme, we control the two-dimensional (2D) motion of a free electron using a two-color field to probe the atoms from different angles. We present a new theoretical analysis that focuses on the spherical symmetry of atomic potentials. We analyze previously presented experimental results (Shafir *et al* 2009 *Nat. Phys.* **5** 412–6) and demonstrate the ability to distinguish between spherically symmetric (s state) and non-spherically symmetric (p state) orbitals. Finally, we discuss the limitations of our approach and compare it with alternative methods.

[5] Author to whom any correspondence should be addressed.

Contents

1. Introduction

Particle collisions are the main tool for investigation of the structure of matter. Recently, it has been demonstrated that the strong laser-field-assisted recollision of electron and ion can reveal structural information about the atomic or molecular wavefunction [2]–[5]. In this process, the laser field first removes an electron from an atom, and then accelerates it to high velocities before it recollides with the parent ion [6]. The recollision leads to the emission of optical radiation in the extreme ultraviolet (XUV) regime with attosecond duration (1 as $= 10^{-18}$ s) [7]. Attosecond pulses are induced by the interference between the electron scattering state and the initial bound state. Therefore, their optical properties encode the spatial information of the two wavefunctions, which thus becomes obtainable. This capability was first demonstrated by Itatani *et al* [8] in a concept entitled 'molecular tomography'. In this approach, a molecule is aligned in the laboratory frame by a pump pulse [9] followed by an ionization–recollision process induced by a second pulse. The high harmonic generation (HHG) spectra collected for a series of molecular alignment angles is used to reconstruct the highest occupied molecular orbital (HOMO), in this case the N_2 σ_g. Recently, it has been demonstrated that measurements of the spectral phase [10] and the spectral polarization [11] provide a sensitive identification of the orbital 'fingerprint', and are thus crucial steps towards its full reconstruction.

The primary limitation of this method is that the sample and probe degrees of freedom are strongly coupled. It has been impossible to manipulate the probe without affecting the sample. In all cases the recolliding electron is correlated with the quantum states from which it ionized. However, the released electron may originate from several orbitals. This occurs in the case

of degeneracy (noble gas atoms) or in molecules where several valence orbitals lying closely below the HOMO may participate in the process [12]. In addition, the ionized states can also depend on the molecular alignment angle [13]. The ionization probability in N_2 does not change significantly with molecular alignment. Therefore, in this case, such a coupling does not present a major limitation. These difficulties have limited the extension of molecular tomography to other molecular systems. Such extension requires separate control of the probing degrees of freedom that will allow probing of structured molecules or molecules that are difficult to align. Furthermore, it will allow the probing of atomic wavefunctions that cannot be aligned by means of standard techniques.

In our recent paper [1], we presented a new approach to control the probing angles by manipulating the electron two-dimensional (2D) trajectory using a two-color field. We applied this approach experimentally and demonstrated the ability to distinguish between a spherically symmetric wavefunction (s state in helium atoms) and a non-spherically symmetric wavefunction (p state in neon atoms). Applying a plane wave approximation to describe the continuum electron, we analyzed the measured data and concluded that the probed state in neon corresponds to an almost pure $mi = 0$ p state, where mi is the angular momentum projection on the laser field axis.

In this paper, we present a complete and detailed description of our probing scheme presented in [1]. While the previous paper presented the general scheme, here we take an important step forward in the theoretical analysis of the method. We rely on the spherical symmetry of atomic potentials, which enables the separation between the radial and the angular properties. Such separation reduces the dimensionality of the measurement. Furthermore, it allows us to probe the atomic wavefunction without relying on a specific model to describe the recolliding electron. We theoretically derive the recollision step using a scattering waves model and link the symmetry of the orbital to the polarization of the emitted harmonics.

This paper presents a complete and self-contained description of our new approach. Initially, we theoretically derive the recollision in atomic wavefunctions. Next, we summarize the experimental results presented in [1] and compare them to the theoretical prediction. Finally, we discuss the limitations of our technique and present alternative approaches.

2. Controlling the angle between ionization and recollision

The proposed method for separating between the ionization and the probing degrees of freedom relies on the manipulation of the laser field's polarization. A simple approach is to add ellipticity to the linearly polarized field [14, 15]. After ionization, the electron is driven by the laser field, while the orthogonally polarized component of the field deflects it in the lateral direction. Since the electron is born with a finite transverse momentum, it recollides with the parent ion with a reduced probability [16]. Increasing the ellipticity will increase the relative angle between ionization and recollision while decreasing the recollision probability. This approach has recently been demonstrated experimentally and will be discussed in a separate paper [17].

A more controllable approach is to add the second harmonic, orthogonally polarized to the linearly polarized fundamental field [18]–[21]. Since the two-color field's periodicity equals one cycle of the fundamental field, the interaction can be analyzed on a single cycle level (see equation (1)). By controlling the intensity of the second-harmonic field and its phase relative to the fundamental field, we achieve a high degree of control over the 2D dynamics of the free

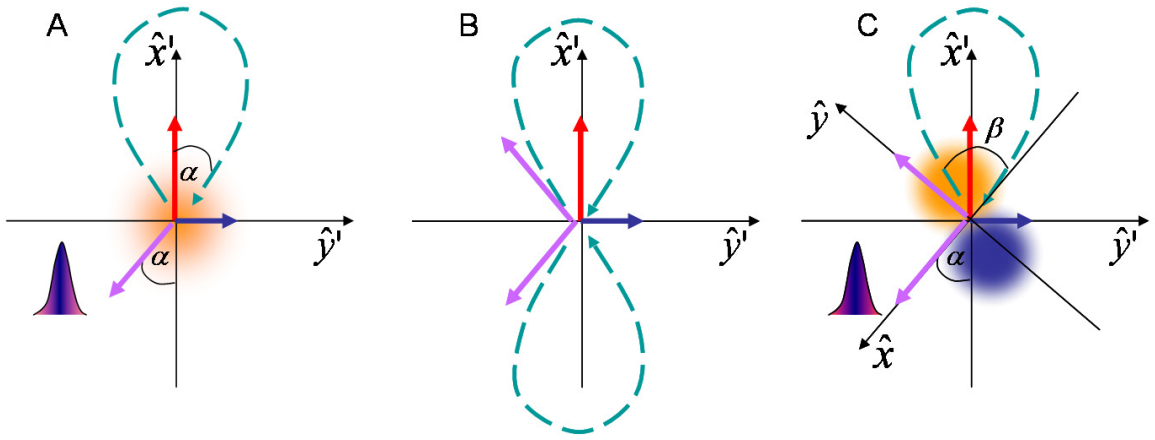

Figure 1. Schematic drawings of HHG in the two-color field. (A) Spherically symmetric orbital. The red and blue arrows correspond to the fundamental and second-harmonic fields in the laboratory frame ($\hat{x}'$, $\hat{y}'$), respectively. Recollision with the ion occurs at an angle α. XUV emission is indicated by a purple arrow and is polarized along the recollision angle. (B) HHG from two adjacent optical half cycles. The motion in the x'-direction is reversed, whereas the y'-component maintains its direction. (C) Recollision with a p state. The angle β is defined as the angle between ionization and recollision. The probing is read in the free electron's frame ($\hat{x}$, $\hat{y}$). The XUV polarization is composed of two vectorial components, polarized along $\hat{x}$ and $\hat{y}$, respectively.

electron. Such control enables the decoupling between the ionization and the probing directions and manipulates their relative angle (see figure 1(A)).

The excursion of the free electron is strongly influenced by the transversal field changing the motion from straight line oscillations to a 2D trajectory in the polarization plane of the laser field. The polarization of the emitted radiation is dictated by the symmetry properties of the bound state and by the recollision angle of the free electron.

From this point, we will focus on the theoretical and experimental analysis of the two-color approach. An analysis and comparison with the elliptically polarized field approach are described in section 6. HHG in the two-color field is generated by a multicycle pulse (30 fs). When the recollision process is induced with linearly polarized light, it occurs every half optical cycle. Due to the symmetry of the interaction, the different pulses interfere constructively for the odd harmonics and destructively for even harmonics of the fundamental field frequency. The addition of the second-harmonic field breaks the symmetry between adjacent half cycles, while symmetry between adjacent full cycles is preserved. The symmetry breaking leads to the generation of even harmonics. Due to the periodicity of the two-color field, the analysis can be performed on a single cycle level. The spectral polarization $\vec{S}(N\omega_0)$ of a harmonic order N arising from the interference between contributions of adjacent half cycles is described as

$$\vec{S}(N\omega_0) \propto [E]_{x'}\hat{x}' + [E]_{y'}\hat{y}' - \mathrm{e}^{-\imath N\pi}([E]_{x'}\hat{x}' - [E]_{y'}\hat{y}') = \begin{cases} 2[E]_{x'}\hat{x}' & \text{for odd } N, \\ 2[E]_{y'}\hat{y}' & \text{for even } N, \end{cases} \tag{1}$$

where $[E]_{x',y'}$ are the dipole transition matrix elements along $\hat{x}'$ and $\hat{y}'$ (defined in the laboratory frame) and ω_0 is the fundamental frequency. The first two terms in equation (1) correspond to the dipole moment induced by the first half cycle field, whereas the last two terms correspond to the dipole moment induced by the second half cycle field. Equation (1) relies on the symmetry of the interaction and holds for any symmetry of the bound state. The process induced by the first half cycle is identical to the process induced by the second half cycle inverted across the y'-axis. This is correct as long as we do not pre-excite the bound state (as is the case in molecular alignment). According to equation (1), odd and even harmonics are orthogonally polarized. If the pulse's spectrum changes slowly as a function of the harmonic number, then the interference between adjacent half cycles projects the x'-component of the polarization vector into the odd harmonics, whereas the y'-component is projected into the even harmonics. An analysis of the symmetry breaking between adjacent half cycles has been described in [22] for parallel polarized fields.

In summary, the addition of an orthogonally polarized field allows the 2D manipulation of the electron's trajectory, and therefore of the relative angle between ionization and recollision. The two-color scheme provides an additional advantage, serving as an effective polarization measurement.

At this stage, we have described the manipulation of the free electron dynamics. In the following stage, we focus on the other part of the electronic wavefunction: the hole left behind after the ionization. The hole structure is dictated by the tunneling mechanism [23]. Tunnel ionization is highly selective, choosing the highest occupied orbitals due to exponential dependence on the binding energy. Furthermore, it selects those orbitals whose wavefunction is greater along the direction of the electric field. For example, the p orbital that lies along the instantaneous electric field axis ($mi = 0$) is considerably more likely to ionize than those lying along the orthogonal directions ($mi = \pm 1$) [24, 25]. Therefore, quantum state selection can be viewed as an effective alignment of the atomic wavefunction.

The three-step process is dictated by two important angles. The first angle is α, the recollision angle defined as the angle between the electron momentum vector at recollision and the polarization of the fundamental field. The second angle is β, defined as the angle between the polarization of the field at the time of ionization and the recollision direction (see figure 1(C)). If the orbital's quantization axis is selected by the tunneling process, β serves as the effective probing angle of the orbital. Obviously, the free electron cannot be accurately described by one momentum component but rather by a wavepacket whose spatio-temporal evolution is governed by the time-dependent Schrödinger's equation. We simplify the analysis by assuming that both the asymptotic value of the free electron's momentum and the ionization direction follow the classical trajectory.

We define two different reference frames. One is the previously described laboratory frame (x', y') in which the laser polarization vectors are defined. The second frame is defined by the direction in which the free electron recollides with the ion. We define this direction as the x-axis, while the y-axis is perpendicular to x. This recollision frame rotates as a function of the harmonic order, intensities and phases of the laser fields. This frame is rotated from the laboratory frame by an angle α.

The probing parameters are well defined not in the laboratory frame but in the frame of the recolliding electron. The vector components of the dipole moment $\vec{E}$ in this frame, parallel and perpendicular to the free electron momentum $\vec{k}$, are described as

$$[E(\vec{k}, \beta)]_x = \langle \Psi_g(\beta)|x|\Psi_c(\vec{k})\rangle, \qquad [E(\vec{k}, \beta)]_y = \langle \Psi_g(\beta)|y|\Psi_c(\vec{k})\rangle, \tag{2}$$

where $\Psi_g(\beta)$ is the pre-selected orbital, aligned along β, and $\Psi_c(\vec{k})$ is the continuum wavefunction with momentum $\vec{k}$. Since β is defined relative to x, $\beta = 0$ is the recollision axis. The second-harmonic field influences the symmetry of Ψ_c. However, in the vicinity of the ion, Ψ_c is assumed to be an even function of y. This approximation holds for the high-frequency range but becomes invalid for the low-frequency range. Therefore, if the orbital is spherically symmetric, the integral for $[E]_y$ vanishes. In this case, a dipole moment will be induced along the recollision direction, producing high harmonics polarized along the x-axis. Thus, if the orbital is spherically symmetric, the HHG process provides a direct measurement of the recollision angle. When introducing more structured orbitals, the symmetry of the recombination is broken, leading to dipole oscillations along both the x-axis and the y-axis. Such symmetry breaking can be observed by measuring the polarization of the emitted light, resulting in rotation of the polarization vector from the x-axis. Since a two-color scheme provides a direct measurement of the polarization vector (see equation (1)), we will apply it in the following in order to distinguish between spherically symmetric and non-spherically symmetric wavefunctions.

3. Polarization state of atomic dipole emission

When analyzing the high harmonic polarization from wavefunctions that are not spherically symmetric, we need to examine the recollision process more thoroughly. In the following section, we will derive the vectorial properties of the dipole moment in the recollision frame and then link the derivation to observable parameters in the laboratory frame. We begin by considering an atomic radial potential $V(r)$. Both the bound and unbound solutions to Schrödinger's equation have a separable form:

$$\Psi_{n/k,l,m}(r,\theta,\varphi) = \chi_{n/k,l}(r)\cdot Y_l^m(\theta,\varphi), \tag{3}$$

where $\chi_{n/k,l}(r)$ is a radial function and $Y_l^m(\theta,\varphi)$ is the spherical harmonic. n, l and m are the principal, angular momentum and its projection quantum numbers, respectively. The unbound (continuum) states are indicated by a field free momentum k defined at infinity and pointing along $\hat{x}$. The recombination spectrum from the continuum state $\Psi_c(\vec{k}) = \sum_{l',m'} B_{l',m'}\Psi_{k,l',m'}$ to the ground state $\Psi_{n,l,m}$ results in a photon with an energy of $\epsilon = \frac{k^2}{2} + Ip$, where Ip is the ionization potential. The recombination spectrum is defined as

$$\begin{aligned}\vec{S}_{n,l,m}(\vec{k}) &= C(k)\sum_{l',m'} B_{l',m'}\langle\Psi_{n,l,m}(\vec{r})|\vec{r}|\Psi_{k,l',m'}(\vec{r})\rangle \\ &= C(k)\sum_{l',m'} B_{l',m'}\langle\chi_{n,l}(r)|r|\chi_{k,l'}(r)\rangle\langle Y_l^m(\theta,\varphi)|\hat{r}|Y_{l'}^{m'}(\theta,\varphi)\rangle,\end{aligned} \tag{4}$$

where $B_{l',m'}$ are the continuum state expansion coefficients and $C(k)$ reflects unknown quantities, such as the transversal amplitude of the continuum wavefunction and the detection efficiency. Since the recollision is approximated to occur on the x-axis, defined beforehand as the electron frame, we choose it as the quantization axis and neglect all continuum terms with nonzero m'. The total angular momentum quantum number is restricted as well by the selection rule $l' = l \pm 1$. We start by solving the angular integrals and consider their vector components.

3.1. Spherically symmetric orbital

In the simplest case of a spherically symmetric orbital, the integral is reduced to

$$\begin{aligned}[S(\vec{k})]_x &\propto \langle Y_0^0(\theta,\varphi)|\sin(\theta)\cos(\varphi)|Y_1^x(\theta,\varphi)\rangle,\\ [S(\vec{k})]_y &\propto \langle Y_0^0(\theta,\varphi)|\sin(\theta)\sin(\varphi)|Y_1^x(\theta,\varphi)\rangle.\end{aligned} \tag{5}$$

The notation $Y_1^x(\theta,\varphi)=\frac{1}{2}\sqrt{\frac{3}{\pi}}\sin(\theta)\cos(\varphi)$ denotes a p state polarized along the x-axis defined in the (x, y) frame. As noted above, the integral for $[S]_y$ vanishes.

3.2. Non-spherically symmetric orbital

In the case of a p orbital rotated by an angle β from the x-axis, the integrals take the following form:

$$\begin{aligned}[S(\vec{k},\beta)]_x &= C(k)\langle Y_1^x(\theta,\varphi-\beta)|\sin(\theta)\cos(\varphi)|B_{0,0}A_{k,0}Y_0^0(\theta,\varphi)+B_{2,0}A_{k,2}Y_2^x(\theta,\varphi)\rangle\\ &= C(k)\cos(\beta)\left(B_{0,0}A_{k,0}\frac{1}{\sqrt{3}}+B_{2,0}A_{k,2}\frac{2}{\sqrt{15}}\right),\\ [S(\vec{k},\beta)]_y &= C(k)\langle Y_1^x(\theta,\varphi-\beta)|\sin(\theta)\sin(\varphi)|B_{0,0}A_{k,0}Y_0^0(\theta,\varphi)+B_{2,0}A_{k,2}Y_2^x(\theta,\varphi)\rangle\\ &= C(k)\sin(\beta)\left(B_{0,0}A_{k,0}\frac{1}{\sqrt{3}}-B_{2,0}A_{k,2}\frac{1}{\sqrt{15}}\right),\end{aligned} \tag{6}$$

where $A_{k,l'}$ denote the radial integrals. The ratio of the spectral vector components becomes

$$\frac{[S(\vec{k},\beta)]_y}{[S(\vec{k},\beta)]_x}=\tan(\beta)\frac{B_{0,0}A_{k,0}\frac{1}{\sqrt{3}}-B_{2,0}A_{k,2}\frac{1}{\sqrt{15}}}{B_{0,0}A_{k,0}\frac{1}{\sqrt{3}}+B_{2,0}A_{k,2}\frac{2}{\sqrt{15}}}=\Gamma(\vec{k})\tan(\beta). \tag{7}$$

By calculating the ratio, we eliminate the dependence on the unknown function $C(k)$ and are left with a structure function that depends on the electron momentum $\Gamma(\vec{k})$ times an angular function. The separability of the wavefunctions is reflected in the separability of the spectral ratio. The overall symmetry of a noble gas closed p electronic shell is spherically symmetric. However, during tunnel ionization, this symmetry is broken due to a greater probability of the $mi=0$ states tunneling through the barrier. Here, mi is defined as the quantum number for angular momentum projection on the laser polarization. It is important to note that, during the laser cycle, the reference frame is rotating. Thus, each tunneling instant defines a different quantization axis that is correlated to the recollision axis of the same electron.

The perfect selectivity assumption results in a $\tan(\beta)$ angular dependence of the spectral ratio (equation (7)). If we relax the requirement for perfect selectivity, we reach different angular functions of the form

$$\frac{[S(\vec{k},\beta)]_y}{[S(\vec{k},\beta)]_x}=\Gamma(\vec{k})\frac{\sin(\beta)+a\cos(\beta)}{\cos(\beta)+a\sin(\beta)}, \tag{8}$$

with a being the ionization probability ratio for the orthogonal p state, which in turn can depend on the sub-cycle electric field or polarization. We see that, by measuring the spectral ratio,

we obtain information about the selectivity achieved by the tunneling process. Information regarding the radial part of the wavefunctions can be obtained from $\Gamma(\vec{k})$ as well.

3.3. Spectral ratio measured in the laboratory frame

How can we extract the spectral ratio $\frac{[S]_y}{[S]_x}$ from the experimental measurement? Our experiment measures the projection of the polarization components in the laboratory frame (x', y'). However, we do not have access to their relative phase δ. In section 6.2, we suggest a method to measure this phase. If the relative phase is either known or measured, then we can directly transfer the measurement from the lab frame to the electron frame:

$$\frac{[S]_y}{[S]_x} = \frac{[S]_{x'}\sin(\alpha) - e^{i\delta}[S]_{y'}\cos(\alpha)}{[S]_{x'}\cos(\alpha) + e^{i\delta}[S]_{y'}\sin(\alpha)}, \tag{9}$$

where α is the recollision angle. The frame transformation relies on the calibration of α using a spherically symmetric orbital, as discussed in section 5.1. Such calibration assumes that the continuum dynamics (and therefore α) is mostly governed by the generating field's configuration and not by the bound state structure.

The spectral ratio is extremely sensitive to the spatial symmetry of the orbital. Assuming that the continuum wavefunction is an even function in the vicinity of the ion, we can detect the symmetry of the bound state without relying on a specific recombination model, such as the plane wave approximation or a scattering approach, which requires additional information of the atomic potential [26, 27].

4. Numerical and experimental procedures

4.1. Simulation procedure

We simulate the HHG process by a laser field composed of 800 and 400 nm components in orthogonal polarizations with an intensity ratio of 3 : 1. We define the ionization axis for each moment of ionization, t_0, according to the instantaneous direction of the electric field. Correspondingly, for every t_0 we define a spread of initial momenta in the orthogonal direction to the ionization axis. These definitions set the initial conditions of the free electron's motion. Next, the free electron propagates in space and time according to the Newtonian equations of motion neglecting the Coulomb potential. The spread in the momentum space defines a group of electron trajectories. One trajectory is finally selected by demanding a closed trajectory. The selected trajectory defines the calculated recollision momentum (k) and recollision angle (α). The calculated events are separated into long trajectories and short trajectories according to their chirp direction. In the scope of this work, we will consider only short trajectories, since in the experiment these are selected spatially by propagation effects. The simulation procedure was carried out for a range of red–blue delays.

4.2. Experimental procedure

High harmonics are generated with 30 fs, 50 Hz, 2 mJ, 800 nm laser pulses in an atomic gas jet. We estimate the pulse intensity to be $\sim 1.8 \times 10^{14}\,\mathrm{W\,cm^{-2}}$ according to the cut-off harmonic. The second-harmonic field with an intensity ratio of 3 : 1 is produced using a 100 μm type-I BBO (BaB_2O_4) crystal. The second-harmonic field is orthogonally polarized with respect to

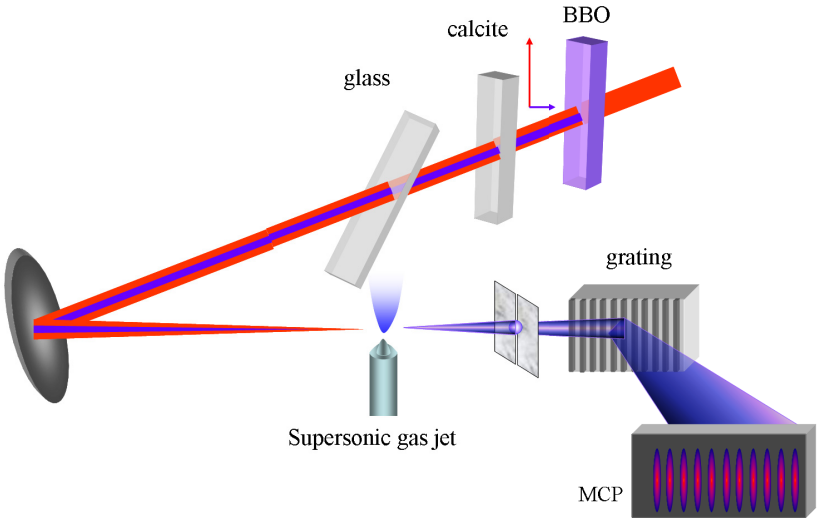

Figure 2. Schematic illustration of the experimental setup.

the fundamental field. Group-velocity dispersion is compensated using a birefringent crystal (calcite). The relative phase of the second-harmonic field relative to the fundamental field is controlled with 250 μm of BK7 glass. High harmonics are generated by focusing the two beams into a pulsed gas jet. A thin ($\sim$1 mm) gas jet is used in order to avoid phase mismatch, so we effectively measure the single-atom response [28]. The two colors do not have exactly the same focusing conditions and temporal profile. Therefore, the intensity ratio changes both in time and in space. However, due to the high ionization potential, only the central part of the pulse contributes to the generated harmonics. The harmonic spectrum is measured by an XUV spectrometer. The experimental setup is illustrated in figure 2.

5. Experimental results analysis

In the following section, we discuss in detail the experimental results, first presented in [1], and compare them to the numerical simulations.

5.1. Measuring α, the recollision angle

As suggested by equation (2), the recollision angle can be directly extracted by measuring HHG from a spherically symmetric orbital. As described in section 3.3, such a measurement is essential to link the recollision frame to the laboratory frame. We extract the angle experimentally by producing HHG from helium probing its 1s state. The high harmonic spectrum as a function of red–blue delay is shown in figure 3. Various features appear in the spectrum; the most dominant ones are the dark areas on the sides of the picture. The low signal measured for these values of red–blue delay appears due to the lateral shift of the recolliding electron from the parent ion, leading to low recollision probabilities. The most important feature observed in the helium spectrum is the interplay between odd and even harmonics. In the low-energy regime, only even harmonics appear, whereas in the high-energy limit, only odd harmonics are observed. We previously stressed the correspondence of the harmonic parity to

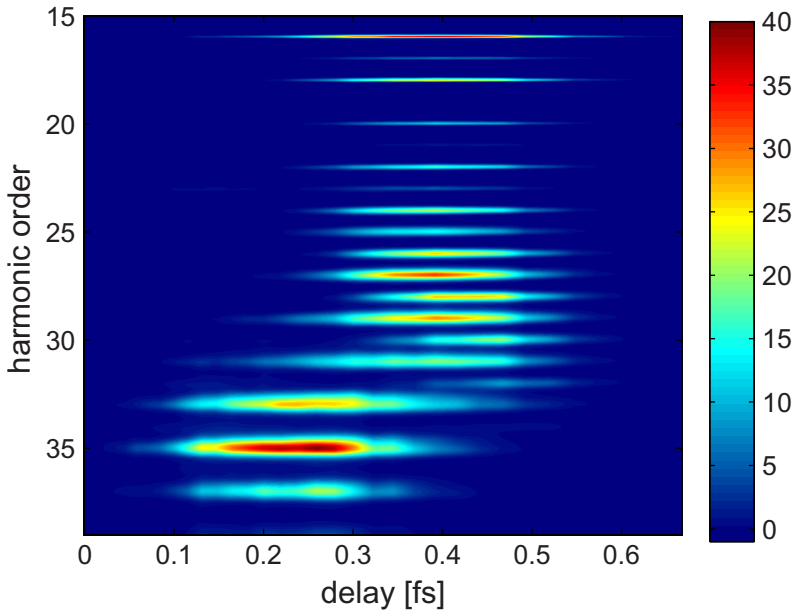

Figure 3. High harmonic spectrum from helium atoms as a function of the delay between red and blue fields (false color scale).

the polarization, and in turn to the recollision angle. The first stage in analyzing the harmonic spectrum is to separate the even and odd harmonic orders, and by that to obtain two spectra of orthogonal polarizations. Then, relying on the fact that there are no sharp transitions or electronic resonances in this spectral regime, we interpolate the spectrum between adjacent harmonics and create a continuous spectrum. The ratio between the square roots of the two spectra corrected for detector efficiencies for the different polarizations gives a measurement of the polarization angle's absolute value (see figure 4(A)). If the highest occupied orbital is spherically symmetric, like the helium 1s, the harmonic polarization angle reflects the free electron's recollision angle according to

$$|\alpha(N,\tau)| = \arctan\left(\sqrt{\frac{I(\text{even N},\tau)}{I(\text{odd N},\tau)}}\right), \tag{10}$$

where $I(\text{even N})$ and $I(\text{odd N})$ are the even and odd harmonic intensities, respectively, N the harmonic order and τ the two colors' delay. A plot of the simulated recollision angle is shown in figure 4(B) (low probability events are filtered). We observe that, in the high-energy range, the recollision angle approaches zero in both the experiment and the calculation. In contrast, in the low-energy region, the experimental results deviate strongly from the calculations and approach 90°. We relate this deviation to a small, imperfect overlap of the two-color field. While the high-energy harmonics are generated by the most intense cycles within the pulse duration at the central part of the beam, low-energy harmonics are also generated by the lower intensity wings of the pulse in time and in space, and therefore are more influenced by such averaging. In addition, as mentioned in section 2, our analysis relies on a classical description of the electron trajectory, and on its symmetry around the recollision axis, which is less accurate in the low-energy range.

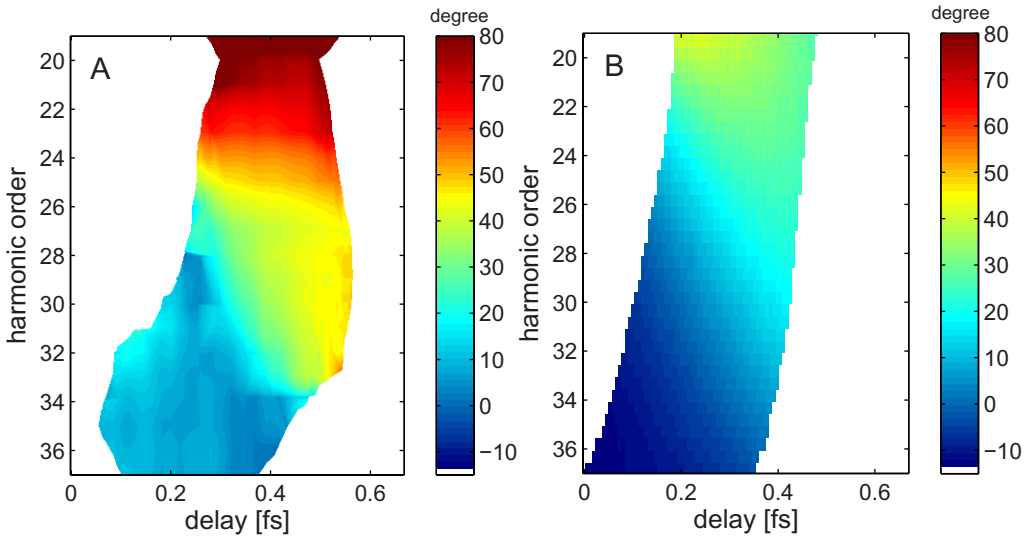

Figure 4. Recollision angle α. (A) Measured from the helium spectrum. (B) Obtained by simulation. The general trend of low recollision angles at the high-energy region appears both in experiment and in the simulation. At the lower-energy regime the experimental angle climbs faster than the simulated one.

5.2. Probing a non-spherically symmetric wavefunction

In the following stage, we perform the two-color measurement with neon atoms. The harmonic spectrum is displayed in figure 5(A). Comparing this measurement with the helium measurement, we observe a close similarity of the dark region structures. Since the dark regions correspond to the displacement of the free electron from the parent ion, it confirms that the continuum dynamics are similar when the generating field configuration is the same. A striking difference between the atomic spectra appears in the high-energy region. Whereas only odd harmonics appeared in the helium spectrum in this regime, here there are equal intensities of even and odd harmonics. This is a clear signature for symmetry breaking induced by the atomic orbital.

Whereas the symmetry breaking of the atomic wavefunction can be directly identified in figure 5(A), extracting its spatial distribution requires a more careful analysis. At this point we encounter two fundamental limitations to our approach. The first limitation is related to the transformation of the frame of measurement. As derived in section 3, we can probe the symmetry of the wavefunction in the free electron's frame. A rotation of the frame requires a measurement of the relative angle between the two frames (the recollision angle) and the relative phase between $[S]_{x'}$ and $[S]_{y'}$. The angle was measured in section 5.1; the relative phase remains unknown. In our previous paper [1], we assumed that the free electron wavefunction is a plane wave. In this case, both polarization components of the dipole are real, and therefore the frame of measurement can be directly rotated. However, in the vicinity of the ionic core, such an assumption becomes invalid and a more accurate model has to be applied. In general, an accurate model that describes the free electron wavefunction is required in order to calculate the relative phase. The absence of this measurement becomes a major limitation to our technique.

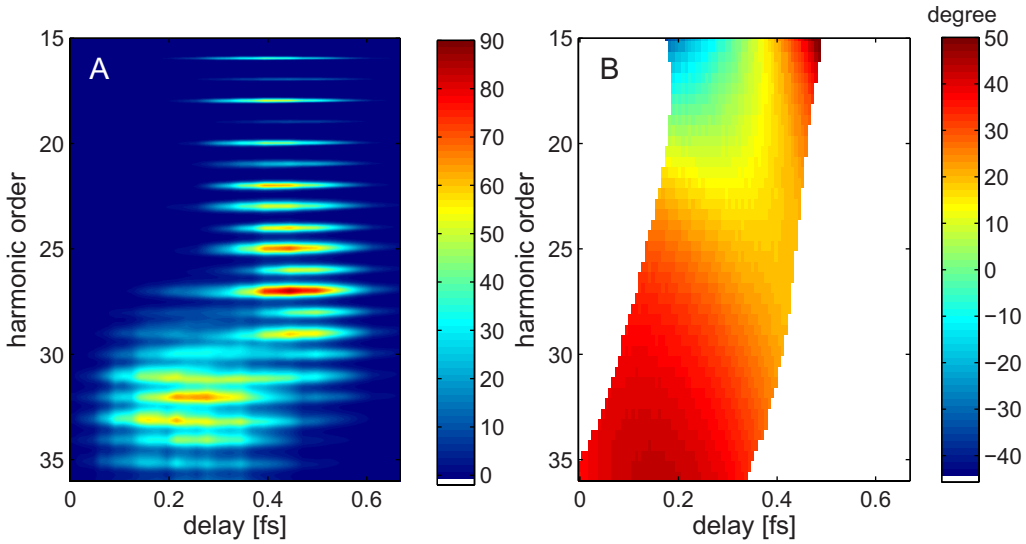

Figure 5. (A) High harmonic spectrum from neon atoms (false color scale). (B) Simulated total probing angle β. Only a limited range of probing angles is obtained for each spectral regime.

The second limitation is related to the limited range of probing angles that can be achieved in our experiment. Figure 5(B) presents the total probing angle (β), derived in the simulation. High values ($>40^\circ$) are obtained in the highest spectral regime. This measurement, however, does not support a wide range of probing angles for each harmonic order. The main limitation is set by the sensitivity of our detection. Our measurement observes electron trajectories that have the maximal probability of recolliding. Enhancing the sensitivity of our detector will allow the detection of events with lower recollision probability, and therefore increase significantly the range of probing angles. In the following sections, we will address both limitations and discuss alternative approaches that overcome them.

6. Extending the measurement technique

6.1. Alternative approaches to probe atomic wavefunctions

In the present experiment, we have used a two-color scheme with a second harmonic in a low-intensity level compared to the fundamental. This enabled selectivity in ionization, control over the free electron and a polarization measurement through separation of odd and even harmonic orders. An additional degree of control is the relative blue field intensity. Scanning the blue field intensity from zero to 25% will provide an angular probing range of about 40° in the high spectral range.

A significant enhancement to the angular probing range can also be achieved by using a weak fundamental beam with a strong second-harmonic beam. Such a combination allows systematic scanning of the probing angles. In this case, the recollision process occurs four times during a full fundamental cycle. Two similar but opposite sign trajectories are induced in the first and third fundamental quarter cycles, and two other similar trajectories are induced in the

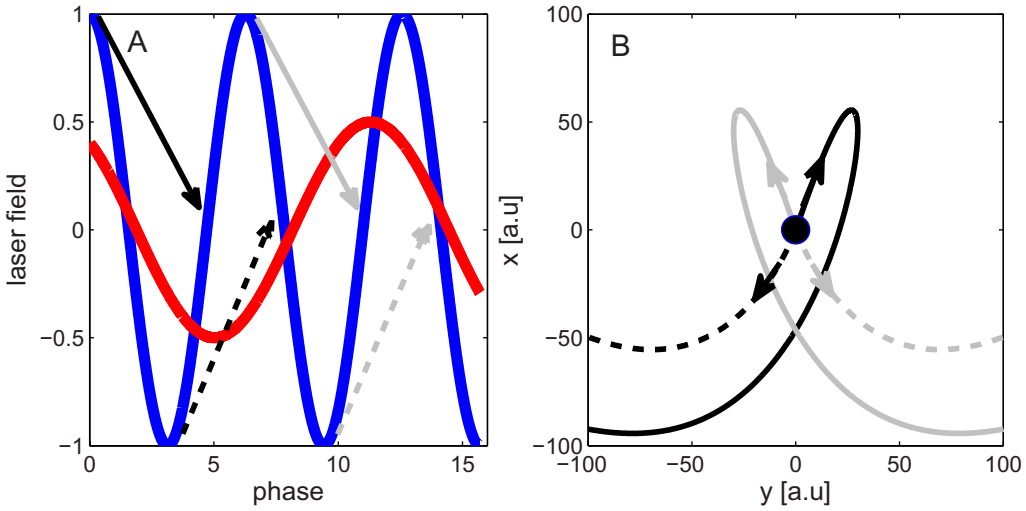

Figure 6. Electron trajectories in the weak fundamental–strong second-harmonic scheme. (A) x-polarized red field on a 20% intensity level of a y-polarized blue field. The four arrows represent different electron trajectories, which are plotted in panel (B). The dashed trajectories drift away from the ion, whereas the solid trajectories have large probabilities of recolliding.

second and fourth fundamental quarter cycles. Examples of such trajectories are illustrated in figure 6.

Only the first family of trajectories have a significant recollision probability, and therefore our analysis will focus on these solutions. The probing angles reached in this scheme are presented in figure 7. As demonstrated in the figure, a wide range of probing angles is reached across the entire HHG spectral range. In this scheme, the polarization of the dipole moment is measured in a manner similar to the measurement described by equation (1). The ability to increase the angular probing range will allow a full characterization of the atomic wavefunction.

6.2. Rotating the frame of measurement from the lab frame to the free electron's frame

Rotation of the frame of measurement requires a measurement of the relative phase between the two orthogonal components of the dipole moment, $[E]_{x'}$ and $[E]_{y'}$. When the two colors have an orthogonal polarization, these two components are separately mapped into odd and even harmonics and therefore their relative phase cannot be measured. We can extend our approach by rotating the blue field's polarization by a small angle. In this case, the electron trajectory induced by the positive half cycle is not a mirror image of the trajectory induced by the negative half cycle, as described in figure 1(B). If the blue field's polarization is rotated by a small angle, we can consider the rotation in a perturbative manner. The small rotation of the field's polarization does not modify the dynamics of the free electron, and the main effect will be a small phase shift σ accumulated by the electron. Positive and negative half cycles will induce opposite phase shifts. A full analysis of the perturbation is beyond the scope of this paper and will be published separately. In this section, we will describe the perturbation in a schematic manner relying on the perturbation analysis applied in [22]. The interference between the two

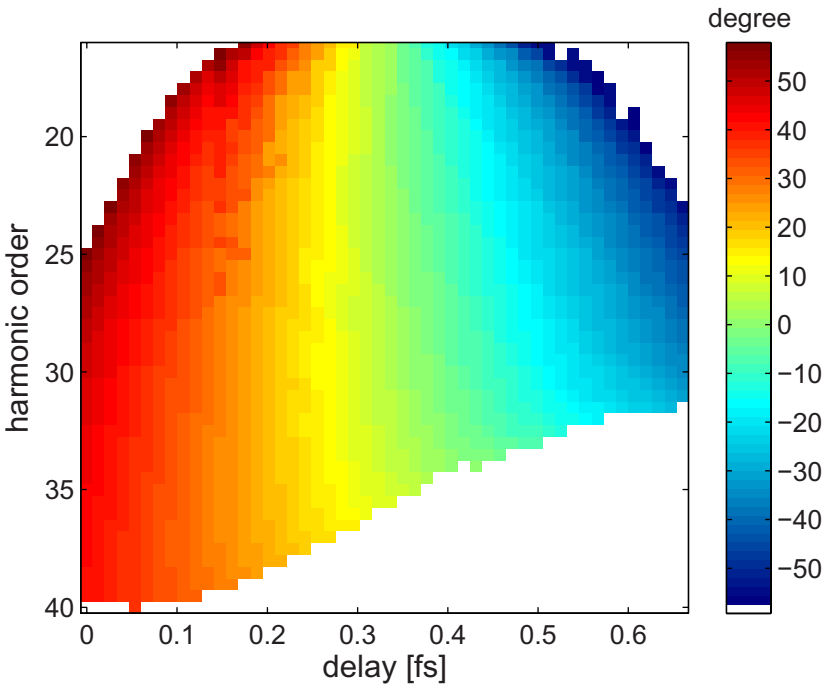

Figure 7. Effective probing angles β reached in the weak fundamental–strong second-harmonic scheme as a function of 800 nm harmonic orders.

half cycles is described by modifying equation (1) to be

$$\vec{E}(N\omega_0) = ([E]_{x'}\hat{x}' + [E]_{y'}\hat{y}')\mathrm{e}^{\mathrm{i}\sigma} - \mathrm{e}^{-\mathrm{i}N\pi}([E]_{x'}\hat{x}' - [E]_{y'}\hat{y}')\mathrm{e}^{-\mathrm{i}\sigma}. \tag{11}$$

In the following step, we transfer the emitted harmonics through a polarizer aligned at 45° with respect to the fundamental beam's polarization. The polarized field can be expressed as

$$\begin{aligned} E(\text{odd N}) &= \sqrt{2}([E]_{x'}\cos(\sigma) - \mathrm{i}[E]_{y'}\sin(\sigma)), \\ E(\text{even N}) &= \sqrt{2}(-\mathrm{i}[E]_{x'}\sin(\sigma) + [E]_{y'}\cos(\sigma)). \end{aligned} \tag{12}$$

A measurement of the polarized field interferes the two field components $[E]_{x'}$ and $[E]_{y'}$, which enables the extraction of their relative phase and therefore the transformation of the frame of measurement.

6.3. High harmonic generation (HHG) with an elliptical field

An alternative approach to manipulate the 2D dynamics of the free electron relies on generating HHG with a single-color elliptically polarized field. This approach is described in detail and experimentally demonstrated in [17]. In this section, we summarize this approach, compare it to the two-color one and link it to the theoretical analysis provided in section 3. A major limitation to this approach is the lack of control of the phase between the longitudinal and transversal fields (as in the two-color scheme), which is fixed at $\pi/2$. The probing angle increases with the ellipticity. However, since the recollision probability decreases as well, the final range of probing angles is limited. The polarization of the field cannot be extracted directly from the measurement, as in the two-color case. Therefore, an XUV polarizer has to be utilized. The

XUV polarizer enables the performance of a full characterization of the field's polarization: the ellipticity ϵ_p and rotation angle η for each harmonic. The transformation of these parameters to the electron frame is straightforward, if we can measure or calculate the angle between the laboratory frame and the electron frame α. In this scheme, the spectral ratio can be rotated to the labratory frame according to

$$\frac{[S]_y}{[S]_x} = \frac{\sin(\eta-\alpha) \pm i\epsilon_p \cos(\eta-\alpha)}{\cos(\eta-\alpha) \mp i\epsilon_p \sin(\eta-\alpha)}. \tag{13}$$

7. Summary and future perspectives

In this paper, we present a complete description of a new approach for probing atomic wavefunctions, which was first discussed in [1]. We describe a new theoretical analysis to probe atomic wavefunctions, utilizing the spherical symmetry of atomic potentials. We analyze the main limitations to our approach and discuss alternative methods. In the future, increasing the angular probing range will enable us to resolve their structural information without relying on an accurate description of the free electron's wavefunction. We measure a field selected state—the atomic wavefunction selected by tunnel ionization. Such a measurement allows us to study the tunneling process itself by changing the main parameters of the interaction, such as laser intensity or fundamental wavelength.

The next challenge would be to retrieve orbital dynamics. If more than one electronic wavefunction interacts with the laser field, then the probed electronic state is not stationary and may evolve during the optical cycle. Since the probed wavefunction is composed of several atomic orbitals, it will no longer be separable. The separability of the wavefunction can easily be detected according to equation (7) by scanning the probing angles. Its modification with the harmonic number will provide direct probing of the evolution of the wavefunction in time.

The proposed model can be applied to resolve the structure of molecular orbitals. By probing randomly aligned molecules, we can study the selectivity of molecular orbitals induced by tunneling ionization. Recently, Niikura *et al* [29] extended this approach to study the outcome of tunnel ionization in N_2, O_2 and CO_2 molecules. We can add an important parameter to the measurement and fix the molecular axis using a molecular alignment scheme. An independent control over the molecular axis will enable us to select various orbitals and probe them independently.

Acknowledgments

Financial support of this research by the Israel Science Foundation, the Crown center and the Minerva Foundation is gratefully acknowledged.

References

[1] Shafir D, Mairesse Y, Villeneuve D M, Corkum P B and Dudovich N 2009 Atomic wavefunctions probed through strong-field light-matter interaction *Nat. Phys.* **5** 412–6

[2] Lein M, Hay N, Velotta R, Marangos J P and Knight P L 2002 Role of the intramolecular phase in high-harmonic generation *Phys. Rev. Lett.* **88** 183903

[3] Vozzi C *et al* 2005 Controlling two-center interference in molecular high harmonic generation *Phys. Rev. Lett.* **95** 153902

[4] Kanai T, Minemoto S and Sakai H 2005 Quantum interference during high-order harmonic generation from aligned molecules *Nature* **435** 470–4
[5] Torres R *et al* 2007 Probing orbital structure of polyatomic molecules by high-order harmonic generation *Phys. Rev. Lett.* **98** 203007
[6] Corkum P B 1993 Plasma perspective on strong field multiphoton ionization *Phys. Rev. Lett.* **71** 1994–7
[7] Paul P M *et al* 2001 Observation of a train of attosecond pulses from high harmonic generatio *Science* **292** 1689–92
[8] Itatani J *et al* 2004 Tomographic imaging of molecular orbitals *Nature* **432** 867–71
[9] Stapelfeldt H and Seideman T 2003 Colloquium: aligning molecules with strong laser pulses *Rev. Mod. Phys.* **75** 543–57
[10] Haessler S *et al* 2010 Attosecond imaging of molecular electronic wavepackets *Nat. Phys.* **6** 200–6
[11] Levesque J *et al* 2007 Polarization state of high-order harmonic emission from aligned molecules *Phys. Rev. Lett.* **99** 243001
[12] Smirnova O *et al* 2009 High harmonic interferometry of multi-electron dynamics in molecules *Nature* **460** 972–7
[13] Pavičić D, Lee K F, Rayner D M, Corkum P B and Villeneuve D M 2007 Direct measurement of the angular dependence of ionization for N_2, O_2 and CO_2 in intense laser fields *Phys. Rev. Lett.* **98** 243001
[14] Budil K S, Salières P, Perry M D and L'Huillier A 1993 Influence of ellipticity on harmonic generation *Phys. Rev.* A **48** R3437–40
[15] Antoine P, Carré B, L'Huillier A and Lewenstein M 1997 Polarization of high-order harmonics *Phys. Rev.* A **55** 1314–24
[16] Dudovich N *et al* 2006 Attosecond temporal gating with elliptically polarized light *Phys. Rev. Lett.* **97** 253903
[17] Shafir D *et al* Origin of elliptically polarized high order harmonics in atoms in preparation
[18] Kitzler M and Lezius M 2005 Spatial control of recollision wave packets with attosecond precision *Phys. Rev. Lett.* **95** 253001
[19] Eichmann H *et al* 1995 Polarization-dependent high-order two-color mixing *Phys. Rev.* A **51** R3414–7
[20] Andiel U, Tsakiris G D, Cormier E and Witte K 1999 High-order harmonic amplitude modulation in two-colour phase-controlled frequency mixing *Europhys. Lett.* **47** 42–8
[21] Kim I J *et al* 2005 Highly efficient high-harmonic generation in an orthogonally polarized two-color laser field *Phys. Rev. Lett.* **94** 243901
[22] Dudovich N *et al* 2006 Measuring and controlling the birth of attosecond xuv pulses *Nat. Phys.* **2** 781–6
[23] Ammosov M V, Delone N B and Kraĭnov V P 1986 Tunnel ionization of complex atoms and of atomic ions in an alternating electromagnetic field *Zh. Eksp. Teor. Fiz.* **91** 2008 (*Sov. Phys.—JETP* **64** 1191–4)
[24] Young L *et al* 2006 X-ray microprobe of orbital alignment in strong-field ionized atoms *Phys. Rev. Lett.* **97** 083601
[25] Loh Z-H *et al* 2007 Quantum state-resolved probing of strong-field-ionized xenon atoms using femtosecond high-order harmonic transient absorption spectroscopy *Phys. Rev. Lett.* **98** 143601
[26] Wörner H J, Niikura H, Bertrand J B, Corkum P B and Villeneuve D M 2009 Observation of electronic structure minima in high-harmonic generation *Phys. Rev. Lett.* **102** 103901
[27] Le A-T, Lucchese R R, Tonzani S, Morishita T and Lin C D 2009 Quantitative rescattering theory for high-order harmonic generation from molecules *Phys. Rev.* A **80** 013401
[28] Levesque J, Zeidler D, Marangos J P, Corkum P B and Villeneuve D M 2007 High harmonic generation and the role of atomic orbital wave functions *Phys. Rev. Lett.* **98** 183903
[29] Niikura H, Dudovich N, Villeneuve D and Corkum P B Mapping molecular orbital symmetry using high harmonic generation spectrum observed by two-color laser fields *Phys. Rev. Lett*. accepted